Experimental Verification of Rudder Control Method Based on Yaw Moment Observer for Electric Skycars in Driving Mode

Sho Umeda[*a)] Student Member, Hiroshi Fujimoto[*] Senior Member
Akira Nishizawa[**] Non-member, Hiroshi Kobayashi[**] Non-member

Skycars can be the ultimate answer to on-demand mobility because they have a driving mode and a flying mode. There is a trade-off between the stability of the driving mode and the performance of the flying mode. However, considering electric skycars, the trade-off can be solved by a control method which takes advantage of the electric motor quick response. The rudder control method for yaw moment disturbance in the driving mode has already been proposed. However, the previous experimental verification was incomplete, therefore further experimental verification is needed. In this paper, the rudder control method for yaw moment disturbance suppression in the driving mode is proposed again and its effectiveness is verified by simulation and experiment.

Keywords: Skycar, Electric airplane, Electric aircraft, Rudder, Yaw rate control

1. Introduction

Recently, skycars have gathered attention and many development cases are reported [(1)~(3)]. In these days, a growing interest is directed towards on-demand mobility [(4)]. Skycars can be the ultimate answer to future on-demand mobility because they have a driving mode and a flying mode.

There is a trade-off between the stability of the driving mode and the performance of the flying mode, and the trade-off needs to be improved. For safety reasons, the skycar should be given more priority to the flying mode. However, an airplane-like skycar is affected heavily by disturbance such as side wind and roughness of the road during the driving mode. Therefore, the aim of this paper is improving the driving stability of the skycar by developing control method.

Many control methods for improving the driving stability of vehicles have been proposed especially for electric vehicles (EVs). Electric motors have the following advantages [(5)].

- The motor torque response is about 100 times faster than that of engines.
- The motor torque is estimated accurately by measuring the motor current.
- Kinetic energy can be regenerated into electric energy.
- The direction of motor torque can be switched seamlessly.
- Dispersed placement and independent control are easier to achieve than in engines.

Many researches for improving flying stability of airplane, such as gust alleviation control, auto landing, and height control have been reported [(6)~(9)].

Control methods for electric airplanes (EAs) such as thrust control and vertical velocity control taking advantages of the electric motor [(10)(11)] have been proposed. Motion control method for electric propulsion ships, which have propellers as well as EAs, has been also proposed [(12)].

Fig. 1. Overview of FPEA1.

However, researches on improving the driving stability of the skycars are not still incomplete. In electric skycars, the trade-off between performance of the flying mode and stability of the driving mode could be resolved using the high control performance of electric motors.

Generally, the front wheel load is very small in order to nose-up when take off. This is the same as airplane-like skycar. If the front wheel is a steering wheel, its reliability is likely to be low. Therefore, yawing control is must be achieved without a steering wheel.

Vertical stabilizers and rudders must be installed to the skycar for yawing control during flying mode. It can also be expected that controlling the rudder can provide yawing control in driving mode.

In this paper, a rudder control method is proposed for yaw moment disturbance suppression in the driving mode. An observer is designed for yaw moment disturbance estimation from yaw rate measurement. Rudders are controlled to sup-

a) Correspondence to: umeda@hflab.k.u-tokyo.ac.jp
* The University of Tokyo
5-1-5, Kashiwanoha, Kashiwa-shi, Chiba, Japan, 277-8561
** Japan Aerospace Exploration Agency
6-13-1, Osawa, Mitaka-shi, Tokyo, Japan, 181-0015

(a) Flying mode. (b) Driving mode.

Fig. 2. Conceptional drawings of FPEA1.

Table 1. Specifications of FPEA1.

Empty weight	118 kg
Length	4.83 m
Wing span	(10.6 m)
Main wing surface area	(10.4 m^2)
Canard wing surface area	(1.4 m^2)
Wheelbase	2.35 m
Height	1.62 m
Battery	Li-Polymer
Propeller diameter	1.50 m
Propeller motor type	20 poles outer rotor SPM
Propeller motor maximum output	21 kW

press the estimated yaw moment disturbance. The effectiveness of the proposed method is verified by simulation and experiment.

2. Experimental airplane

In this section, the characteristics of the experimental airplane, Future Personal Electric Airplane 1 (FPEA1) are described.

2.1 Overview of FPEA1 FPEA1 used for performance verification is shown in Fig. 1. FPEA1 has pusher configuration, whose advantages include broader front sight and smaller drag compared with tractor configuration. The drag of the wing is smaller than that of a tractor configuration airplane because the propeller slipstream does not hit the wing. This makes high speed cruising easier. However, the air-cooling performance is likely to be lower than that of a tractor airplane.

FPEA1 currently doesn't have the wings and the canard. Conceptional drawings are shown in Fig. 2. Flying mode is shown in Fig. 2 (a), driving mode is shown in Fig. 2 (b), during which the wings will be folded. The specifications of FPEA1 are shown in Table 1. The parameters in parenthesis mean specifications under construction. The details of the motor that driving the propeller are reported in (13). The motor has a rotor and two stators. This structure enables airplanes safe landing, even if one stator fails and provides redundancy of the system.

2.2 Wheels Front and rear wheels are shown in Fig. 3. The front wheel is a caster. An encoder of 3600 pulses is equipped on the left rear wheel, and the revolution speed of the wheel can be calculated. The front wheel's load is 2.6 kg, while the rear wheel's load is 115.2 kg. Therefore, it can be inferred that the center of gravity (CoG) of FPEA1 is near the rear wheels.

2.3 Rudder actuators The rudder actuator is shown in Fig. 4. The rudder actuator consists of the servo motor and the ball-screw unit. The actuators steer rudders by pushing and pulling the rods. The specifications of rudder actuators are shown in Table 2.

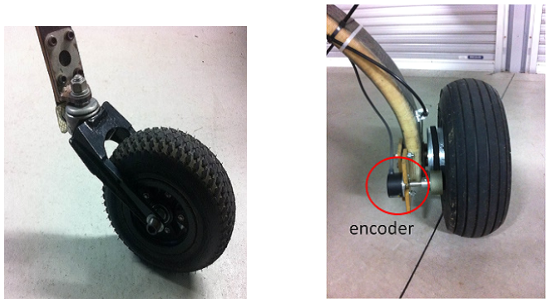

(a) Front wheel. (b) Rear wheel (left one).

Fig. 3. Front and rear wheel.

(a) Overview. (b) Enlarged.

Fig. 4. Rudder actuator (left one).

Table 2. Specifications of the rudder actuators.

Maximum rudder angle	±30 deg
Maximum thrust	470 N
Maximum steering angular velocity	229 deg/s

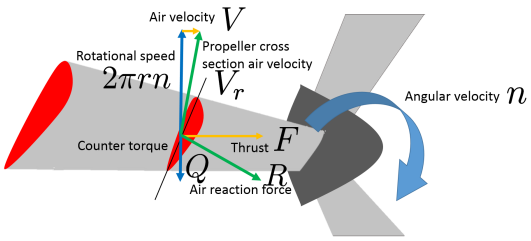

Fig. 5. Physics of propeller.

3. Modeling

3.1 Dynamics of propeller In this section, the dynamics of propeller are described. Fig. 5 shows the overview of the propeller dynamics. A cross section of the propeller blade is an airfoil and takes reaction force R from the air. By resolving R into propulsive direction and rotating direction, propulsive component is thrust F and rotating component is counter torque Q. Thrust F and counter torque Q are expressed as

$$F = F_c(y)\rho D_p^2, \cdots\cdots (1)$$

$$Q = Q_c(y)\rho D_p^3, \cdots\cdots (2)$$

where, D_p is diameter of the propeller, ρ is air density and n is revolution speed of the propeller. F_c and Q_c are dimen-

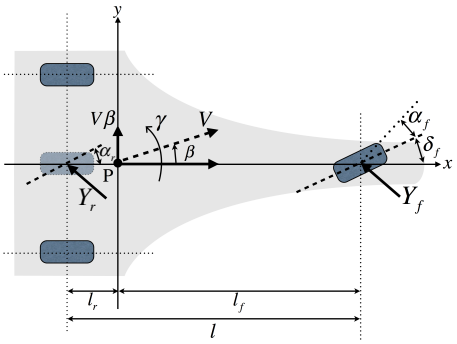

Fig. 6. Three-wheel model.

sionless number and functions of advanced ratio. Advanced ratio y is defined as

$$y = \frac{nD_p}{\max(V, \epsilon)}, \cdots (3)$$

where, V is air speed and ϵ is the infinitesimal constant in order to avoid zero division.

The propeller's equation of rotational motion is expressed as

$$J_\omega \dot{\omega} = T - Q, \cdots (4)$$

$$\omega = 2\pi n, \cdots (5)$$

where, J_ω is the propeller inertia and ω is the propeller angular velocity.

3.2 Longitudinal model The equation of longitudinal motion is expressed as

$$M\dot{V}_E = F - D, \cdots (6)$$

Where, M is the skycar's mass, V_E is ground velocity and D is drag. The relationship between ground speed V_E, air speed V, and tailwind U is expressed as Eq. (7).

$$V = V_E - U. \cdots (7)$$

The drag D is expressed as Eq. (8) using the dimensionless number C_D, called drag coefficient.

$$D = \frac{1}{2} C_D \rho S V^2. \cdots (8)$$

S is the wing surface area.

3.3 Yawing model On the basis of three-wheel model shown in Fig. 6, the equation of motion around z axis can be expressed as

$$I\frac{d\gamma}{dt} = N_t + N_r + N_d, \cdots (9)$$

$$N_t = -C_f\left(\beta + \frac{l_f}{V_E}\gamma\right) l_f + 2C_r\left(\beta - \frac{l_r}{V_E}\gamma\right) l_r. \cdots (10)$$

where, I is the inertia around z axis, γ is the yaw rate, N_t is the moment generated from lateral force of the tire, N_r is the moment generated from rudder steering and N_d is the moment generated from disturbance such as side wind and unevenness of the road. C_f is the cornering stiffness of the front wheel, C_r is the cornering stiffness of the rear wheel, β is the side slip angle of CoG, l_r is the distance between CoG and the front wheel, l_f is the distance between CoG and the rear wheel. Variation of I generated from rudder steering is supposed to be infinitesimal, therefore it can be ignored.

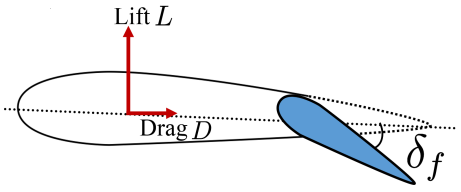

Fig. 7. Lift and drag.

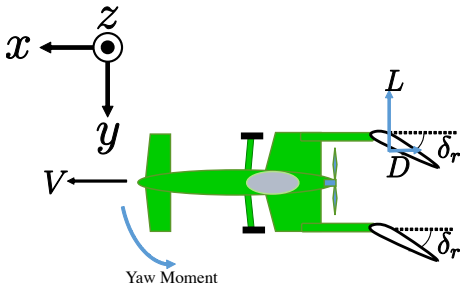

Fig. 8. Relation between rudder and yaw moment.

The equation of lateral motion is expressed as

$$mV_E\left(\frac{d\beta}{dt} + \gamma\right) = Y_f + 2Y_r + Y_d, \cdots (11)$$

$$Y_f = -C_f\left(\beta + \frac{l_f}{V_E}\gamma\right), \cdots (12)$$

$$Y_r = -C_r\left(\beta + \frac{l_r}{V_E}\gamma\right), \cdots (13)$$

where, Y_f is the front wheel lateral force, Y_r is the rear wheels lateral force and Y_d is the lateral force generated from disturbance.

Fig. 7 shows the aerodynamic force lift and drag. While drag has already been shown as Eq. (8), lift is expressed as Eq. (14).

$$L = \frac{1}{2} C_L \rho S V^2. \cdots (14)$$

Here, C_L is a dimensionless number called lift coefficient. C_L is a linear function of flap steering angle δ_f in conditions of not stalling. The overview of the relation between rudder and yaw moment is shown in Fig. 8. Considering the analogy between two sets of relationships, rudder - vertical stabilizer and wing - flap, vertical stabilizer's lift coefficient is a linear function of rudder steering angle δ_r. Increasing the lift coefficient generates yaw moment as illustrated in Fig. 8. Increasing the rudder steering drag leads to yaw moment in the opposite direction of the arrow. Generally, C_L is much larger than C_D. Therefore, rudder steering angle δ_r generates yaw moment as shown in Fig. 8. From the above, yaw moment generated from rudder steering N_r can be expressed as

$$N_r = \frac{1}{2}\rho C_{n\delta_r}(V^2 + w^2)\left(\delta_r - \tan^{-1}\frac{w}{V}\right), \cdots (15)$$

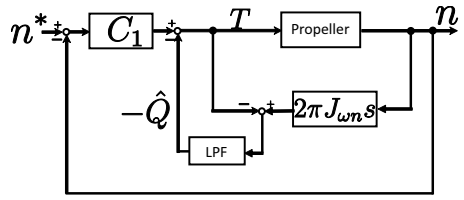

Fig. 9. Block diagram of propeller's revolution controller.

where, ρ is air density, $C_{n\delta_r}$ is the yaw moment coefficient of rudder steering and w is side wind. Thus, yaw moment generated from rudder steering N_r is a monotone increasing function of air velocity V.

Assuming the lateral force created by the caster is negligible, skycar's yawing state space equations expressed in (16) are derived from equation (9)~(15).

$$\begin{cases} \dot{\boldsymbol{x}}(t) = \boldsymbol{A}\boldsymbol{x}(t) + \boldsymbol{B}u(t), \\ \boldsymbol{y}(t) = \boldsymbol{C}\boldsymbol{x}(t), \end{cases} \quad \cdots\cdots (16)$$

Here,

$$\boldsymbol{x}(t) = \begin{bmatrix} \beta \\ \gamma \end{bmatrix}, \cdots\cdots (17)$$

$$u(t) = \delta_r, \cdots\cdots (18)$$

$$\boldsymbol{A} = \begin{bmatrix} \frac{-2}{mV_E} C_r & \frac{-2}{mV_E} C_r \\ \frac{2}{I} C_r l_r & \frac{2C_r l_r^2}{V_E} \end{bmatrix}, \cdots\cdots (19)$$

$$\boldsymbol{B} = \begin{bmatrix} 0 \\ \frac{\rho C_{n\delta_r}}{2I} V^2 \end{bmatrix}, \cdots\cdots (20)$$

$$\boldsymbol{C} = \begin{bmatrix} 0 & 1 \end{bmatrix}. \cdots\cdots (21)$$

4. Controller design

4.1 Design of propeller's revolution speed controller The block diagram of propeller's angular velocity controller is shown in Fig. 9. Propeller's counter torque varies momentarily with changes in angular velocity and advanced ratio y. In order to compensate for the influence of counter torque, counter torque observer (CTO) [10] is adopted. From Eq. (2), Eq. (22) is derived.

$$Q = T - 2\pi J_\omega \dot{n}. \cdots\cdots (22)$$

Given the motor torque T and the revolution speed n, the counter torque can be estimated. CTO is an application of disturbance observer shown in Fig. 9. Supposing the convergence of the motor's current controller is fast enough, The motor torque reference T^* is used instead of motor torque T. The plant is nominalized by adding estimated value of counter torque $\hat{Q}$ in advance. The nominalized plant can be given as Eq. (23).

$$n = \frac{1}{2\pi J_{\omega n}}. \cdots\cdots (23)$$

Here, $J_{\omega n}$ is the propeller nominal inertia. The PI controller is designed with pole placement method based on the nominal plant.

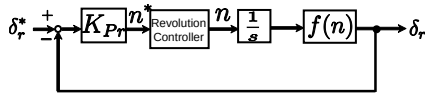

Fig. 10. Block diagram of rudder controller.

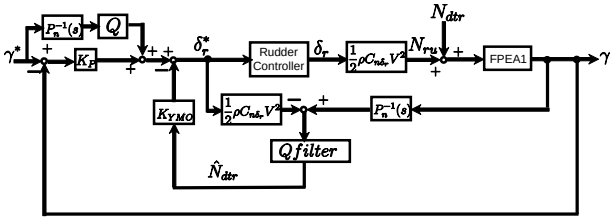

Fig. 11. Block diagram of proposed method.

4.2 Design of rudder controller Rudder controller is designed in outer loop of the motor driver speed controller. Assuming the convergence of motor speed controller is fast enough, the speed control loop can be considered a first order system. $f(n)$ is the transfer function from revolution speed n to rudder angle δ_r. P controller is adopted for rudder controller, and is designed with pole placement method. Ruder controller is shown in Fig. 10.

4.3 Design of yaw rate controller Yaw moment observer(YMO) for yaw rate control of electric vehicles has already been proposed [14]. In this paper, yaw moment observer (YMO) for EVs is applied for yaw rate control of skycars by rudder steering.

The yaw moment generated from rudder steering can be resolved into N_{ru} and N_{rd}, as

$$N_r = N_{ru} + N_{rd} \cdots\cdots (24)$$

$$N_{ru} = \frac{1}{2}\rho C_{n\delta_r} V^2 \delta_r, \cdots\cdots (25)$$

$$N_{rd} = \frac{1}{2}\rho C_{n\delta_r} \times \left\{ -V^2 \tan^{-1}\frac{w}{V} + w^2 \left(\delta_r - \tan^{-1}\frac{w}{V} \right) \right\}, \cdots\cdots (26)$$

where, N_{ru} is the controllable component by rudder steering angle δ_r and N_{rd} is the component generated from disturbance.

YMO estimates N_{dtr} and the sum of N_{rd}, N_t, N_d. The plant is nominalized by adding reference of yaw rate to estimated value of disturbance N_{dtr} in advance. Below the cutoff frequency, the plant is nominalized as Eq. (27).

$$\gamma = \frac{1}{I_n s} N_{ru}. \cdots\cdots (27)$$

The nominal plant $P_n(s)$ is then expressed as Eq. (28) using nominal inertia I_n.

$$P_n(s) = \frac{1}{I_n s}. \cdots\cdots (28)$$

The block diagram of the proposed method is shown in Fig. 11 . Here, Q-filter is a first-order low pass filter with the cutoff frequency of ω_c.

$$Qfilter = \frac{\omega_c}{s + \omega_c}. \cdots\cdots (29)$$

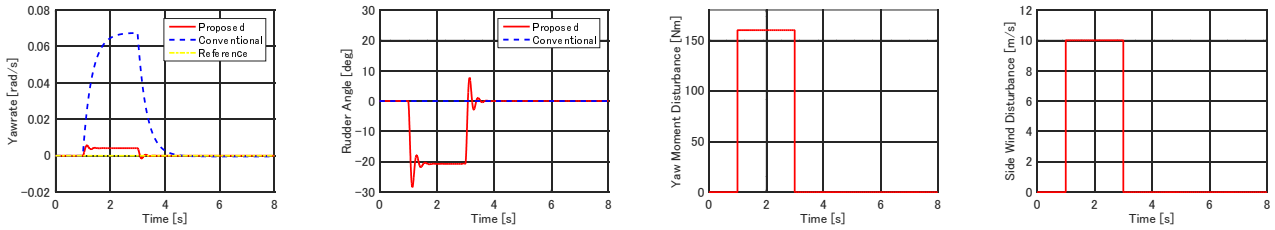

(a) Yaw rate γ (b) Rudder angle δ_r (c) Disturbance yaw moment N_d (d) Disturbance side wind w

Fig. 12. Simulation results.

Table 3. Simulation parameters.

Inertia I	250 kg·m^2
Gross weight M	200 kg
Distance between center of gravity and front wheel l_f	1.57 m
Distance between center of gravity and rear wheel l_r	0.78 m
Cornering stiffness of rear wheel C_r	6040 N/rad
Frontal projected area S_{front}	2.84 m^2
Surface per one rudder S	0.45 m^2
Air velocity V	30 km/h
Side wind disturbance w	10 m/s
Range of rudder angle	± 30 deg
Yawing moment coefficient $C_{n\delta_r}$	3.30×10^{-2}
Cutoff frequency of Q filter	20 rad/s
Gain of YMO K_{YMO}	1.0

5. Simulation

The effectiveness of the proposed method was verified by simulation, comparing the disturbance response with control and without control. It is supposed that skycar is driving at constant velocity V and hit side wind w. Yaw moment disturbance N_d is calculated from side wind w. Without control, rudder steering angle δ_r is constant and equal to zero. Therefore, yaw rate is damped and asymptotic to zero by static stability of the skycar.

The simulation parameters are expressed in Table 3. As shown in Fig. 12(d), 10 m/s side wind disturbance occurs two seconds, one second after the simulation start and lasts two seconds.

It is shown that disturbance response of yaw rate is improved, in comparison with the conventional method shown in Fig. 12(a). Therefore, it is expected that proposed method contribute to achieve driving stability of skycar.

6. Experiment

6.1 Experimental setup and conditions The effectiveness of the proposed method was verified by experiment, comparing the disturbance response with control and without control as well as the simulation. The disturbance yaw moment was generated by treading on the brake pedal of the left rear wheel. The propeller's revolution speed is controlled and is constantly set to 37 rps. In this experiment, the propeller is the only propulsion device. This leads to a decrease of yawing stability because of the asymmetry in rear wheel's load caused by propeller counter torque.

The rudders are steered for controlling yaw rate of the FPEA1 to zero. In other words, zero is input as reference γ^* to the proposed control system shown Fig. 11. Left and right rudders are steered symmetrically in order to generate yaw moment with the same sign.

The brake pedal of the left wheel is tweaked for limiting the excursion and it can be detected reaching the excursion limit (brake flag = 1). The parameters of Table 3 are adopted with exception K_{YMO}, changed to 0.1 in this experiment.

6.2 Experimental results Fig. 13 shows the experimental results. Fig. 13(a), 13(e) show that yaw moment disturbance is generated by pressing the brake pedal. As visible in Fig. 13(d), there is a deference of velocity between the conventional method case and the proposed method case. However, it can be considered allowance because of the following reasons.

- The static stability of FPEA is small enough to be ignored in this speed range.
- The difference of response due to rudder control.

Consequently, the difference doesn't lose fairness of the comparison between conventional method and proposed method cases. Fig. 13(a), 13(b) demonstrate that proposed control system operates correctly.

It is shown in Fig. 13(a) that the disturbance response of yaw rate is improved by applying the proposed method, when compared with the conventional method. Therefore we can say that the proposed method contributes to improve the driving stability of the skycar.

7. Conclusion

In this paper, verification of the yaw rate control method by using rudder is carried out. Good controller performance is proved by simulation and experiment. However, the experimental setup requires further improvement.

In this verification, propeller revolution speed is set to constant. However, setting skycar velocity to a constant value is more desirable. Nevertheless, that would not refute the effectiveness of proposed method.

Future works are improvement of the experimental conditions and the identification the aerodynamic characteristics of the FPEA1 by creating a miniature model. Furthermore, not only yaw rate control, but also yaw angle control is need to be considered.

Acknowledgment

This research was partly supported by the Ministry of Education, Culture, Sports, Science, and, Technology grant (grant number 24249061).

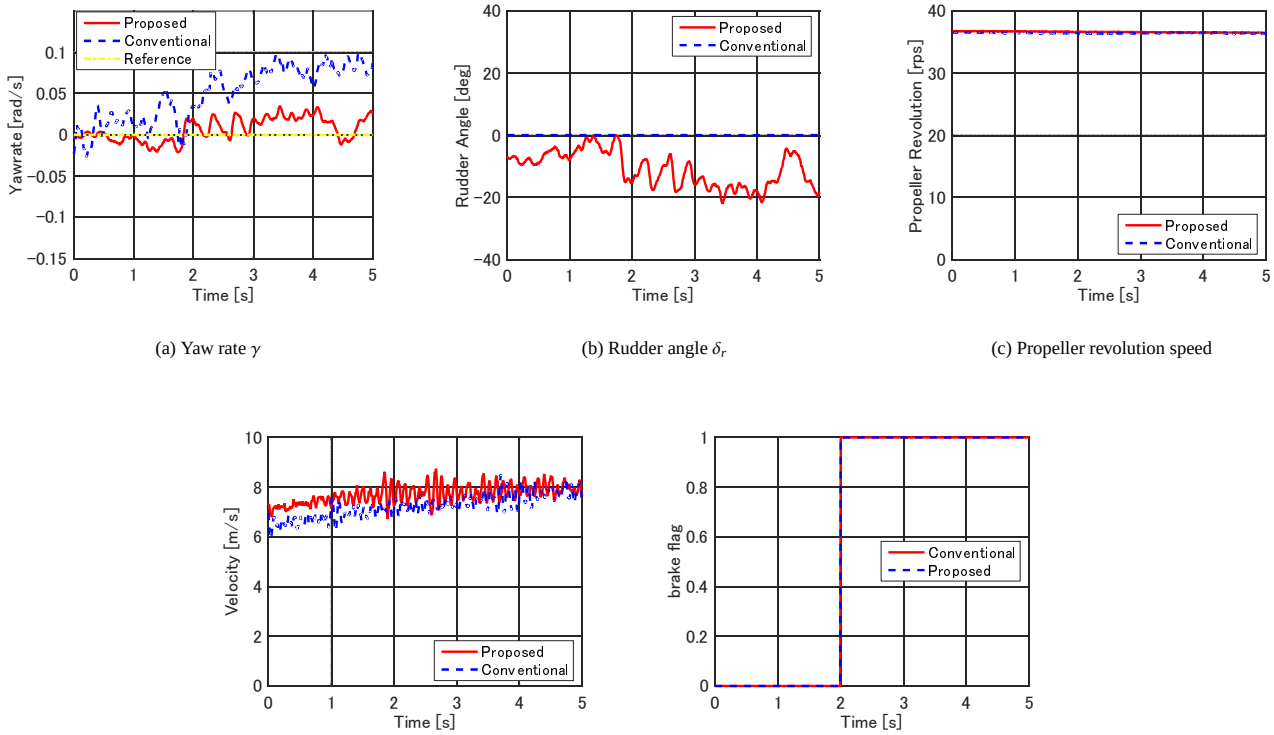

(a) Yaw rate γ (b) Rudder angle δ_r (c) Propeller revolution speed

(d) Velocity V (e) Brake flag

Fig. 13. Experimental results.

References

(1) H. Wax: "Ready for Takeoff," Women in Engineering Magazine, IEEE, Vol. 4, No. 1, pp.14–1, 2010.

(2) moller international: "skycar400," `http://www.moller.com/moller_skycar400.html`, 2016/2/15 accessed.

(3) AeroMobil: "AeroMobil," `http://www.aeromobil.com/`, 2016/2/15 accessed.

(4) Mitchell, W.J. , Borroni-Bird ,C. E. , and Burns, L. D. : "Reinventing the Automobile: Personal Urban Mobility for the 21st Century," The MIT Press (2010).

(5) Y. Hori :"Future Vehicle Driven by Electricity and Control-Research on Four-Wheel-Motored UOT Electric MarchII," IEEE Trans. IE, Vol. 51, No. 5, pp. 954–962, 2004.

(6) M. Sato and N. Yokoyama: "Gust Alleviation Control Using Model Predictive Control-Robustness against Measurement Errors in Prior Turbulence Data and Current State Variables for Aircraft Motions-," Journal of the Japan Society for Aeronautical and Space Sciences, Vol. 59, No. 689, pp. 160–167, 2011. (in Japanese)

(7) L. Coutard and F. Chaumette: "Visual Detection and 3D Model-based Tracking for Landing on an Aircraft Carrier," IEEE International Conference on Robotics and Automation, pp. 1746–1751, 2011.

(8) Y. Sugawara and A. Shimada: "Micro Helicopter Flight Control Using External Sensors," Joint Technical Meeting on "Industrial Instrumentation and Control" and "Mechatronics Control" , IEEJ, IIC-13-56, MEC-13-56, 2013. (in Japanese)

(9) A. Hori, T. Furui, D. Iwakura and K. Nonami :"A Study of Adaptive Control for Multi-rotor Helicopter," , The 12th International Conference on Motion and Vibration, 1C35-1–1C35-9, 2014.

(10) K. Takahashi, H. Fujimoto, Y. Hori, H. Kobayashi, and A. Nishizawa: "Airspeed Control of Electric Airplane Based on 2-Quadrant Thrust Control and Verification with Towing Test Using Electric Vehicle," 40th Annual Conference of the IEEE Industrial Electronics Society, pp. 2682–2688, 2014.

(11) N. Konishi, H. Fujimoto, Y. Watanabe, K. Suzuki , H. Kobayashi, and A. Nishizawa: "Vertical Velocity Control of Electric Airplane by Using Propeller Slipstream for Safe Landing," The 1st IEEJ International Workshop on Sensing, Actuation, and Motion Control, 2015.

(12) R. Yamaguchi, S. Matsuoka, T. Miyazaki, and K. Ohishi: "Motion Control Considering the Thrust Vector of 4-axis Electric Propulsion Ship," Technical Meeting on "Mechatronics Control", IEEJ, MEC-14-170, pp.61–66, 2014. (in Japanse)

(13) H. Kobayashi, A. Nishizawa, K. Okai: "Trend and challenges in electric propulsion systems for aircraft," 49th Aircraft Symposium proceedings, 1C6, pp. 186–191, 2011. (in Japanese)

(14) H. Fujimoto, T. Saito, and T. Noguchi: "Motion Stabilization Control of Electric Vehicle Under Snowy Conditions Based on Yaw-moment Observer," The 8th IEEE International Workshop on Advanced Motion Control 2004, pp. 35–40, 2004.